Available online at www.sciencedirect.com

ScienceDirect

Advances in Space Research 66 (2020) 1775–1791

ADVANCES IN SPACE RESEARCH (a COSPAR publication)

www.elsevier.com/locate/asr

Ionospheric disturbances in a large area of the terrestrial globe by two strong solar flares of September 6, 2017, the strongest space weather events in the last decade

P.R. Fagundes [a,*], M. Pezzopane [b], J.B. Habarulema [c,d], K. Venkatesh [e], M.A.L. Dias [a,f], A. Tardelli [a], A.J. de Abreu [g,h], V.G. Pillat [a], A. Pignalberi [b], M.J.A. Bolzan [i], B.A.G. Ribeiro [a], F. Vieira [a,f], J.P. Raulin [j], C.M. Denardini [f], M.O. Arcanjo [a], G.K. Seemala [k]

[a] *Laboratório de Física e Astronomia, Universidade do Vale do Paraíba (UNIVAP), Av. Shishima Hifumi, 2911, Urbanova, São José Dos Campos, SP, Brazil*
[b] *Istituto Nazionale di Geofisica e Vulcanologia, Via di Vigna Murata 605, 00143 Rome, Italy*
[c] *South African National Space Agency, Space Science, Hermanus, South Africa*
[d] *Department of Physics and Electronics, Rhodes University, Makhanda, South Africa*
[e] *National Atmospheric Research Laboratory (NARL), Gadanki, India*
[f] *Instituto Federal de Tocantins IFTO, Observatorio Fisisica Espacial, Campus Araguatins, TO, Brazil*
[g] *Instituto Tecnologico da Aeronautica, Divisao de Ciencias Fundamentais, Sao Jose Dos Campos, SP, Brazil*
[h] *National Institute for Space Research, 12227-010 S.J. dos Campos, SP, Brazil*
[i] *Departamento de Física, Universidade Federal de Jataí (UFG), Jatai, Goias, Brazil*
[j] *Universidade Presbiteriana Mackenzie, CRAAM, BR-01302907 Sao Paulo, SP, Brazil*
[k] *Indian Institute of Geomagnetism, New Panvel, Navi Mumbai, India*

Received 21 May 2020; received in revised form 23 June 2020; accepted 26 June 2020
Available online 9 July 2020

Abstract

On September 6, 2017, the solar active region AR 2673 emitted two solar flares: the first at 08:57 UT (X2.2) and the second at 11:53 UT (X9.3); both were powerful enough to black-out high and low frequency radio waves (where UT is universal time). The X9.3 was the strongest solar flare event in the past decade. In this study, we took the advantage of these two extreme flare events to investigate corresponding effects on the ionosphere using multi-instrument observations from magnetometers, Global Positioning System – Total Electron content (GPS-TEC) receivers, ionosondes and Swarm satellites over a large geographical extent covering South American, African and European sectors. During the X2.2 flare, European and African sectors were sunlit and during X9.3 European, African, and South American sectors were sunlit and exposed to the solar flare radiation. During the X2.2 flare, there was an ionosonde blackout for a duration of about 45 min, while during the X9.3 flare this blackout lasted for 1 h and 30 min. The blackout are seen over a large global extent which demonstrates the severity of solar flare events in disrupting the radio communication. The horizontal component of Earth's geomagnetic field has shown ripples and enhancements during these flare events. The ionospheric Vertical Total Electron Content (VTEC) showed a positive phase along with an intensification of the Equatorial Ionization Anomaly (EIA) over the South American and African sectors. The dynamical and physical processes associated with the TEC and EIA variabilities due to solar flare are discussed.
© 2020 COSPAR. Published by Elsevier Ltd. All rights reserved.

Keywords: Ionosphere; F-region; Solar flare; EIA

* Corresponding author.
E-mail addresses: fagundes@univap.br (P.R. Fagundes), michael.pezzopane@ingv.it (M. Pezzopane), jhabarulema@sansa.org.za (J.B. Habarulema), maukersdias@ifto.edu.br (M.A.L. Dias), tardelli@univap.br (A. Tardelli), valdirgp@univap.br (V.G. Pillat), alessio.pignalberi@ingv.it (A. Pignalberi), raulin@craam.mackenzie.br (J.P. Raulin), clezio.denardin@inpe.br (C.M. Denardini).

https://doi.org/10.1016/j.asr.2020.06.032
0273-1177/© 2020 COSPAR. Published by Elsevier Ltd. All rights reserved.

1. Introduction

There are growing concerns about the effect of solar flares (SFs) and Coronal Mass ejections (CMEs) on the terrestrial upper atmosphere and ionosphere systems, mainly due to possible deterioration or damage in our communication and navigation satellite systems. Today society is highly dependent on technology involving transfer of data and information via digital means. Therefore, we can define that a new civilization started a new age called digital society and it is unimaginable for a person or a company to be disconnected from communication and navigation systems, even for few hours. Since solar events like SFs and CMEs can produce such kind of damage, space weather becomes one of the most important issues of the new digital society (Berdermann et al., 2018; Yasyukevich et al., 2018; Li et al., 2018; Lei et al., 2018).

An explosion on the Sun´s surface that is originated near a sunspot group in the photosphere or solar chromosphere release a large amount of electromagnetic energy (Zirin, 1988). This kind of space weather event, called a solar flare, release energy in the form of radiations in the entire electromagnetic spectrum. However, the X-ray and EUV (extreme ultraviolet) radiation burst penetrate deeper into the Earth´s atmosphere and will be absorbed in the lower ionosphere (D and E regions) and F-region, respectively (de Abreu et al., 2019; Tsurutani et al., 2005, 2009; Zhang et al., 2017). Also, high energy electrons and protons (from kilo electron volts to hundreds of mega electron volts) are released during some solar explosions and these high energetic particles reach the Earth´s system within half an hour to few hours after the radiation burst (Barta et al., 2019).

Therefore, during solar flares, there is a sudden increase of electron density in the D, E, and F regions of the ionosphere in the hemisphere of the Earth´s atmosphere illuminated by the Sun. These density enhancements are called sudden ionospheric disturbances (SIDs). During solar flares, the intensity of the Equatorial Eletrojet (EEJ) increases along with an increase in the F region electron density leading to an intensification of the equatorial ionospheric anomaly (EIA) (Liu et al., 2004, 2006). In addition, the ionograms recorded by ionosondes may show total or partial blackout, which means that the radio wave pulse transmitted by ionosonde was absorbed by the D-region and there are no echo traces for hours. The radio-waves transmitted by ionosondes (1 to 20 MHz) are absorbed by ionospheric free electrons when the transmitted frequency matches with the plasma frequency, and then the absorbed energy can be re-radiated if this energy is not lost due to collisional frequency or recombination. However, when the D-region increases its electron density, the plasma frequency in this region increases as well and the energy will be absorbed by the neutral atmosphere, via collisional interaction (Barta et al., 2019, Curto et al., 2018, Liu et al., 2006, Sahai et al. 2007).

On September 6, 2017, the solar active region AR 122,673 produced two consecutive solar flares that were powerful enough to block-out high and low frequency radio waves. The first SF (X2.2) erupted from 08:57 UT to 09:10 UT and the second SF (X9.3) erupted at 11:53 UT and reached its maximum at 12:02 UT (Yan et al., 2018). As stated in Bruno et al. (2019) the X9.3 event has been the largest soft X-ray flare since 2006, i.e., for more than a decade. This SF event generated strong white-light emission (de Castro et al., 2018) and multiple heliosesmic waves and was accompanied by an intense and complex radio emission with interplanetary types II-IV bursts and by a long duration of γ-ray emission. More details about γ-ray emission during this event can be found in Lysenko et al. (2019) and Li et al. (2020).

The X9.3 was the strongest SF event in a decade and disturbed the ionosphere in the Earth´s sunlit side. In this study, we took advantage of the two extreme SF events, X2.2 and X9.3, to investigate the effects on the ionosphere using magnetometer networks, Vertical Total Electron Content (VTEC) inferred using GPS dual-frequency receivers, ionosonde and Swarm satellite data. During the SF X2.2 and X9.3 events, the north hemisphere at high-latitude, North America's east sector, South America, Africa, Europe, and Asia were on the sunlit side and directly exposed to the SF radiations (EUV and X-ray, See Fig. 1).

The main objective of the present investigation is to study the ionospheric response from equatorial to mid/high latitudes during the SFs X2.2 and X9.3 over three different regions of the Earth (South America, Africa and Europe) using multi-site and multi-instrument observations. The response of the Earths' magnetic field, the ionospheric VTEC and consequent changes in the Equatorial Ionization Anomaly (EIA) are presented. The importance of multi-instrument and multi-site observations for understanding the global-scale impacts of space weather events is also discussed. This study demonstrates the importance of the use of collocated and simultaneous ground and satellite based observations over different regions of the globe to investigate the global ionospheric response to the space weather events like solar flares and the subsequent impacts on the radio wave applications. Therefore, international scientific programs based on multilateral collaborations are very important to carry out similar kind of investigations.

2. Observations and data analysis

Fig. 1 shows illuminated (bright) and non-illuminated (dark) regions by the solar radiation on the Earth's global maps during two SF events on September 06, 2017 at 09:10 UT and 12:02 UT respectively. The first solar flare was designated as X2.2 class while the second flare is more intense and termed as X9.3. During the first SF event (X2.2) the high latitudes of the northern hemisphere, Europe, Africa, and Asian sectors were illuminated. However, during the second SF event (X9.3) the high latitudes of the northern hemisphere, Latin America, the east sector of USA/

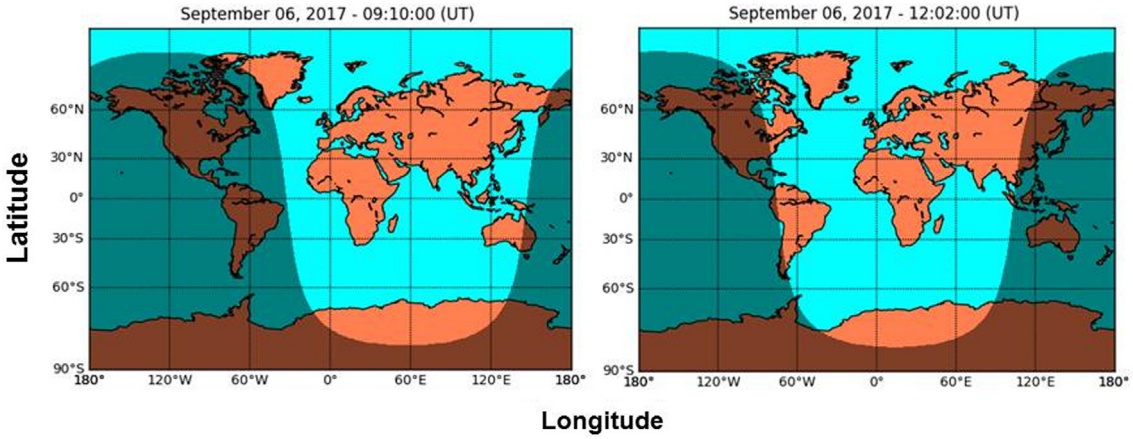


Fig. 1. Global maps showing the geographical extents of Earth´s atmosphere illuminated (bright area) and not illuminated (shaded area) by the Sun at 09:10 UT during the X2.2 SF event (left panel) and at 12:02 UT during the X9.3 SF event (right panel).

Canada, Africa, Europe, and Asian sectors were illuminated. These SFs happened during geomagnetic quiet conditions and the SF X9.3 was the strongest event of the last decade.

Fig. 2 shows the daily variations of geomagnetic index (Dst and Kp), velocity and proton density of solar wind, the interplanetary magnetic field Bz component, X-ray flux observed by GOES satellite, and EUV flux from September 05 to September 07, 2017. It is clear from this figure that the day of SF events, September 06, 2017 was a typical quiet geomagnetic day. During the two SFs, the Dst and Kp indices were around 19 and 16 nT and 1+, and 3−, respectively. Besides, the interplanetary medium was quiet without any significant change. The solar wind speed, proton density and IMF Bz were varying between 450 and 460 km/s, 3.8 and 4.5 protons/cm^{3}s, and 3.8 and −6.2 nT, respectively as seen in Fig. 2A. On the other hand, Fig. 2B shows that on September 06, 2017, the X-ray intensities in both channels 0.05–0.40 nm (blue line) and 0.10–0.80 nm (red line) were strongly disturbed.

The X-ray intensity increases rapidly during the beginning of the SF X2.2 event, followed by an intensity valley between both SFs events. After the second X-ray peak (SF X9.3) the X-ray intensity decreases monotonically. The EUV flux daily variations were obtained from the empirical model of the Flare Irradiance Spectra Model (FISM) (http://lasp.colorado.edu/lisird/). The EUV flux variations are available from 0.1 nm to 190 nm with a wavelength resolution of 10 nm and a 1-minute time cadence. The model is based on a satellite experiment onboard the Thermosphere Ionosphere Mesosphere Energetics and Dynamics (TIMED)/ Solar Extreme ultraviolet Experiment (SEE). More details about this model can be found in Chamberlin et al. (2007, 2008, 2018), and Qian et al. (2011). The contour plot in Fig. 2C shows the EUV flux (W/m^2 Δλ) daily variation as a function of UT and wavelength during September 05–06, 2017. The EUV flux was disturbed in several wavelength channels during both SF events on September 06, 2017. In addition, it is important to mention that the disturbance in EUV flux persisted for nearly 4 h after the occurrence of the strong X9.3 SF event.

The observations from Fig. 2 indicate that the two extreme SF events occurred during quiet geomagnetic conditions with simultaneous strong disturbances in X-ray and EUV fluxes, providing a unique opportunity to investigate the sole impact of SFs on the Earth's ionosphere. Therefore, we have analyzed multi-site observations from different instruments of ground- and satellite-based experiments during these SFs. The ground-based observations of the geomagnetic horizontal component (H), from a network of magnetometers recorded in the Brazilian and African sectors, are used to verify the magnetic field variations. Networks of GPS-TEC and ionosonde data recorded in Brazilian, African and European sectors are also used. In addition, in-situ electron density variations over the South American and African regions measured by the Swarm satellite constellation (Friis-Christensen et al., 2006, 2008) are also analyzed. This collection of different observations are used to investigate in detail the ionospheric response over a large area of the terrestrial globe due to the two strong SFs. Details of considered magnetometers, GNSS receivers, and ionosondes in the three sectors are given in Tables 1–3, respectively.

2.1. Geomagnetic field variations over the Brazilian and African sectors during the solar flares

The horizontal component of the geomagnetic field (H) measured over 10 stations (5 in Brazil and 5 in Africa), are analyzed to compute ΔH variations using the relation $\Delta H(t) = H(t) - H_Q(midnight\ LT)$, where H(t) is the daily variation of the observed horizontal component, and H_Q (midnight LT) is the average of 5 quiet days at local midnight (Denardini et al., 2018).

Fig. 3 shows the diurnal variations of ΔH during September 05 and 06, 2017 over different stations in the Brazilian and African sectors as listed in Table 1. For better visibility

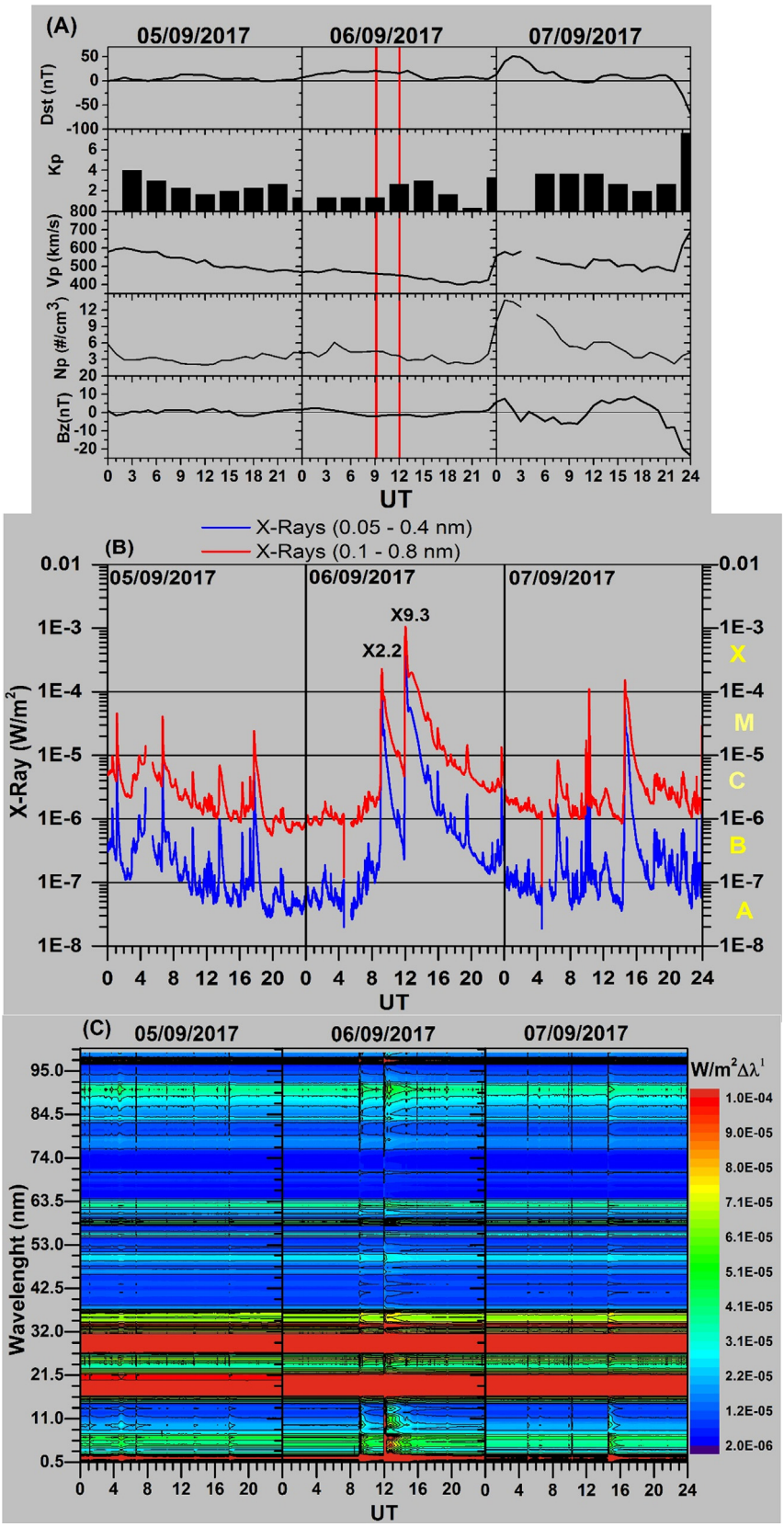


Fig. 2. (A) Daily variations of the geomagnetic indices (Dst and Kp), solar wind speed (Vp), proton density per cm3 (#/Np), and IMF Bz component, from September 5, 2017 to September 7, 2017. The red vertical lines indicate the time of the occurrence of two SF events X2.2 (first line) and X9.3 (second line), respectively. (B) X-ray flux observed by GOES satellite from September 5, 2017 to September 7, 2017. The intensity is shown in wavelength ranges from 0.05 to 0.4 nm (blue line) and from 0.1 to 0.8 nm (red line). Also, on the right side of the Y-axis (yellow) is shown the classification of SFs according to the intensity (A, B, C, M, and X). (C) Contour plots of UV and EUV flux in the wavelength range from 1 to 100 nm from September 5, 2017 to September 7, 2017. (For interpretation of the references to colour in this figure legend, the reader is referred to the web version of this article.)

Table 1
Magnetometer station names, codes, geographic coordinates and dip-latitudes over the Brazilian and African sectors.

Magnetometer Station Name	Station Codes	Geo. Lat. (+N)	Geo. Lon. (+W)	Dip. Lat. (+N)
		Brazilian Sector		
Belem	BEL	−01.4	48.4	−00.5
Araguatins	ARA	−05.6	48.7	−04.1
Eusebio	EUS	−03.9	38.4	−08.4
Cuiaba	CUI	−15.6	56.1	−08.9
Cachoeira Paulista	CXP	−22.7	45.0	−20.5
Magnetometer Station Name	Station Codes	Geo. Lat. (+N)	Geo. Lon. (+W)	Dip. Lat. (+N)
		African Sector		
Tamanrasset	TAM	22.8	−05.5	14.4
Mbour	MBO	14.4	17.0	04.2
Tsumeb	TSU	−19.2	−17.6	−39.1
Hartebeesthoek	HBK	−25.9	−27.7	−41.9
Hermanus	HER	−34.4	−19.2	−45.9

Table 2
GPS-TEC station names, codes, geographic coordinates and dip-latitudes over the Brazilian, African, and European sectors.

GPS Station Name	Station Codes	Geo. Lat. (+N)	Geo. Lon. (+W)	Dip. Lat. (+N)
		Brazilian West Sector		
Porto Velho	POVE	–8.7	63.9	0.3
Colorado d'Oeste	ROCD	–13.1	60.6	–4.8
Barra do Garcas – UFMT	MTGA	–15.9	52.3	–11.1
Dourados – UFGD	MSDR	–22.2	54.9	–14.9
Alegrete	RSAL	–29.8	55.8	–20.2
		Brazilian East Sector		
Belem	BELE	–1.4	48.5	–0.5
Sobral	CESB	–3.7	40.3	–7.1
Vitoria da Conquista	BAVC	–14.9	40.8	–16.9
Ilheus	BAIL	–14.8	39.2	–17.8
Vitoria	CEFE	–20.3	40.3	–21.5
GPS Station Name	Station Codes	Geo. Lat. (+N)	Geo. Lon. (+W)	Dip. Lat. (+N)
		African East Sector		
Djibouti	DJIG	11.5	–42.8	4.9
Malindi	MAL2	–3.0	–40.2	–13.2
Arusha	OLO7	–2.8	–35.9	–13.8
Dodoma	DODM	–6.1	–35.4	–18.2
Mtandika	MTDK	–7.3	–36.3	–19.8
Matola	MATL	−9.6	−34.6	–22.7
Mbamba bay	MBBC	–11.2	–34.7	–24.8
Zomba	ZOMB	–15.4	–35.3	–29.8
Thohoyandou	TDOU	–22.9	–30.5	–39.0
Hermanus	HNUS	–34.4	–19.2	–45.8
GPS Station Name	Station Codes	Geo. Lat. (+N)	Geo. Lon. (+W)	Dip. Lat. (+N)
		European Sector		
Katavia	KATC	36.0	–27.8	32.6
Luzzi	LUZZ	39.4	–16.3	35.7
Ankara	ANKR	39.9	–32.8	37.8
Baku	BAKU	40.4	–49.8	39.8
Ganja	GANJ	40.7	–46.4	39.9
Simeiz	CRAO	44.4	–33.9	43.1
Kiev	GLSV	50.4	–30.5	49.3
Kurchatov	KRTV	50.7	–78.6	54.1
Riga	RIGA	56.9	–24.1	55.6
Kirkkonummi	MET3	60.2	–24.4	58.8

of features, ΔH variations after each SF event are elaborately presented in small frames inside each panel.

We note that after the X2.2 SF (September 06, 2017 from 09:00 to 12:00 UT) ΔH for all stations in the African

Table 3
The ionosonde station names, geographic coordinates along with the start and end time of the fadeout due to X2.2 SF and X9.3 SF.

Ionosonde Stations	Geog. Lat.	Geog. Lon.	SF X2.2 Start Absorption (UT)	SF X2.2 End Absorption (UT)	SF X9.3 Start Absorption (UT)	SF X9.3 End Absorption (UT)
			Brazilian sector			
Araguatins	05.6°S	48.0°W	No	No	12:00	12:30
Jatai	17.9°S	51.7°W	No	No	12:00	13:00
S. J. Campos	23.2°S	45.9°W	No	No	12:00	13:05
			African sector			
Madimbo	22.4°S	30.9°E	09:15	09:45	12:00	13:00
Louisvale	28.5°S	21.9°E	09:15	09:45	12:00	13:00
Grahamstown	33.3°S	26.5°E	09:15	09:45	12:00	13:00
Hermanus	34.4°S	19.2°E	09:00	09:15	12:00	12:45
			European Sector			
San Vito	40.6°N	17.8°E	9:15	9:30	12:00	13:30
Roquetes	40.8°N	00.5°E	9:05	9:50	12:00	13:45
Rome	41.8°N	12.5°E	9:00	9:45	12:00	13:15
Pruhonice	50.0°N	14.6°E	9:15	9:45	12:00	13:30
Dourbes	50.1°N	04.6°E	9.05	9:45	12:00	13:30
Fairford	51.7°N	01.5°W	9:15	9:45	12:00	13:30
Moscow	55.5°N	37.3°E	9:15	10:00	12:00	12:45

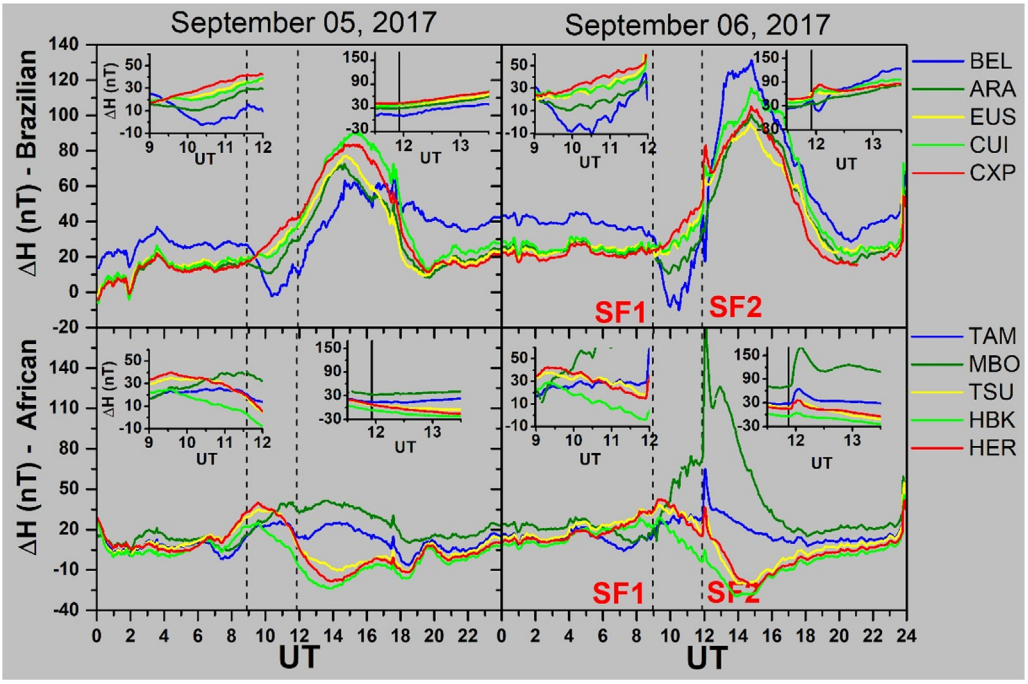


Fig. 3. Daily variation of the magnetic ΔH component observed at BEL, ARA, EUB, CUI, and CXP (Brazilian sector) and TAM, MBO, TSU, HBK, and HER (African Sector) on September 05 and 06, 2017. The flares time are indicated by dashed lines for both days. Also, the ΔH variations are highlighted between 09:00–12:00 and 11:30–13:30 inside of each panel.

and Brazilian sectors show ripple features (see left side small frames for 09:00 UT to 12:00 UT over Brazilian and African sectors) that are not seen during the quiet day (September 05, 2017). It is very interesting to notice in these small frames that the Brazilian sector was not illuminated during the X2.2 SF event (see Fig. 1), but ripples were seen in the ΔH recorded in all Brazilian stations and these ripples (small and continuous fluctuations in the magnetic field for few hours) are similar to those recorded in the African sector. This suggests that solar quiet (S_q) current system have similar minor disturbances in the Earth illuminated and non-illuminated regions during the solar flare.

On the other hand, the X9.3 SF produced significant ΔH disturbances in both sectors. In the Brazilian stations located at low-latitudes (EUS, CUI, and CXP) ΔH presents a peak, and at near-equatorial region (BEL and ARA) a valley is noticed. In the African sector the ΔH peak is

observed at stations located at low-mid latitudes (TAM, TSU, HBK, and HER) as well as near the equatorial region (MBO). Since the African sector was illuminated during both SFs events, it is possible to notice that the ΔH disturbances due to the X9.3 SF are much larger than the disturbances due to the X2.2 SF. This is an indication that the sudden positive ionospheric disturbances produced by the X9.3 yielded large S_q current system disturbances in the Brazilian and African sectors. The changes can be noticed in Fig. 3 comparing the daily variation of the ΔH on September 05, 2017 (quiet day) and September 06, 2017 (disturbed day) from 12:00 UT to 20:00 UT.

As mentioned by Bagiya et al. (2018) the X9.3 SF produced an intense E region ionization over Indian sector and the EEJ current increased ~500% as compared with previous quiet day. The changes observed in the Brazilian and African sectors are in agreement with those reported by Bagiya et al. (2018). Unfortunately, in the Brazilian and African sectors we do not have magnetometers located in the required locations (near and off the geomagnetic equatorial locations) to evaluate the EEJ intensity. However, we can see that the enhancement in ΔH after the X9.3 SF is large at near-equatorial stations (BEL, Brazil and MBO, Africa) when compared to the other stations, which indicates that the EEJ must have significantly enhanced after X9.3 SF over the Brazilian and African sectors.

2.2. GPS and ionosonde observations over the Brazilian, African and European sectors during the solar flares

The GPS measured TEC variations as a function of UT over 10 Brazilian, 10 African, and 10 European stations are presented in Fig. 4A, 4B and 4C respectively. TEC values are computed using the observations from satellites above 30° of elevation. The black and red curves are the observed VTEC mean diurnal variation using 5 quiet days (September 1 to 5, 2017) and during the disturbed day by

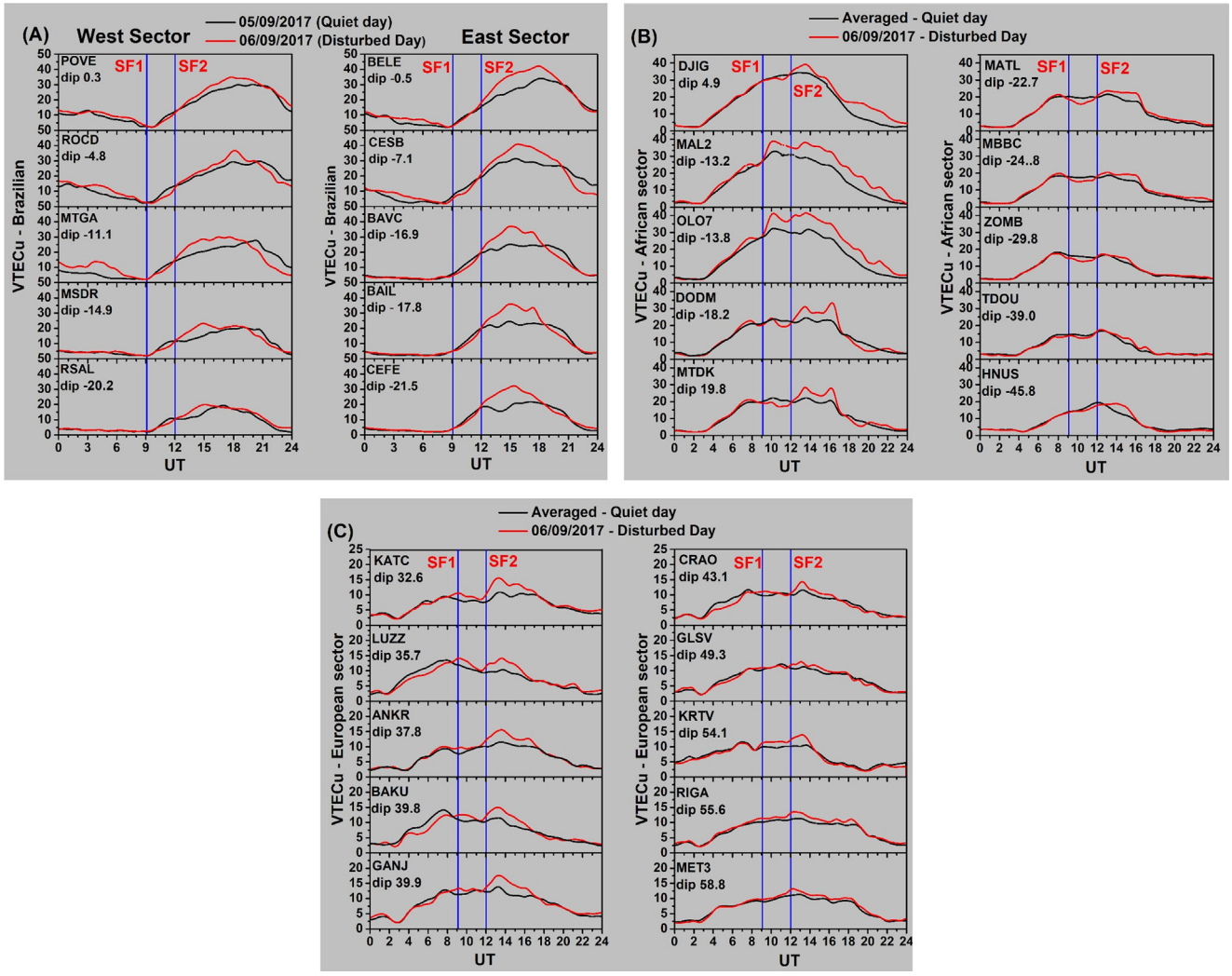


Fig. 4. (A) The comparison of VTEC between quiet (black curves) and SF disturbed day (red curves) over 10 Brazilian stations. (B) The same as (A) but for African sector. (C) The same as (A) but for European sector. (For interpretation of the references to colour in this figure legend, the reader is referred to the web version of this article.)

the two SFs (hereafter SF day, September 06, 2017), respectively. The two blue vertical lines show the time when SFs occurred, where the first line corresponds to the X2.2 SF and the second line to the X9.3 SF. The VTEC daily variations of the quiet mean and flare day are plotted in the same frame to allow a comparative study between quiet and SF conditions. Since the VTEC has latitudinal dependence, the Y-axis for the Brazilian range from 0 to 50 TECu, and African sectors range from 0 to 45 TECu and Y-axis, while for the European sector, TEC ranges from 0 to 25 TECu. For more details about GPS-TEC sites and coordinates used in this investigation see Table 2.

2.2.1. The ionospheric VTEC and ionosonde response due to the X2.2 solar flare

The first SF took place at 08:57 UT (X2.2) and during this first event, the Brazilian ionosphere was not illuminated by sunlight (Fig. 1, left panel) and hence it is not disturbed. This is evident in Fig. 4A where VTEC values from 09:00 UT to 12:00 UT during disturbed and quiet times are quite similar. Further, the ionograms snapshots obtained at 08:45 UT (before the X2.2 SF) and 09:15 UT (after the X2.2 SF) over the Brazilian sector are presented in Fig. 5A. It can be noticed from the ionogram recorded over Araguatins at 09:15 (Fig. 5A-right panel) that the E and F echoes are very clear indicating that there is no radio frequency wave absorption in the Brazilian sector due to the X2.2 SF.

On the other hand, European and African sectors are illuminated by this first SF event X2.2 and the ionosphere is disturbed in both sectors. As seen from Fig. 4B, in the African sector, at near-equatorial region (dip-latitude 4.9°N) and between dip-latitudes from 18°S to 45°S, VTEC values are approximately 3% and 10% lower than those of the quiet period, respectively. However, near dip latitude of 13°S, VTEC values during the disturbed time are approximately 18% higher than those of the quiet period (Fig. 4B). The observed VTEC behavior during this first SF in the

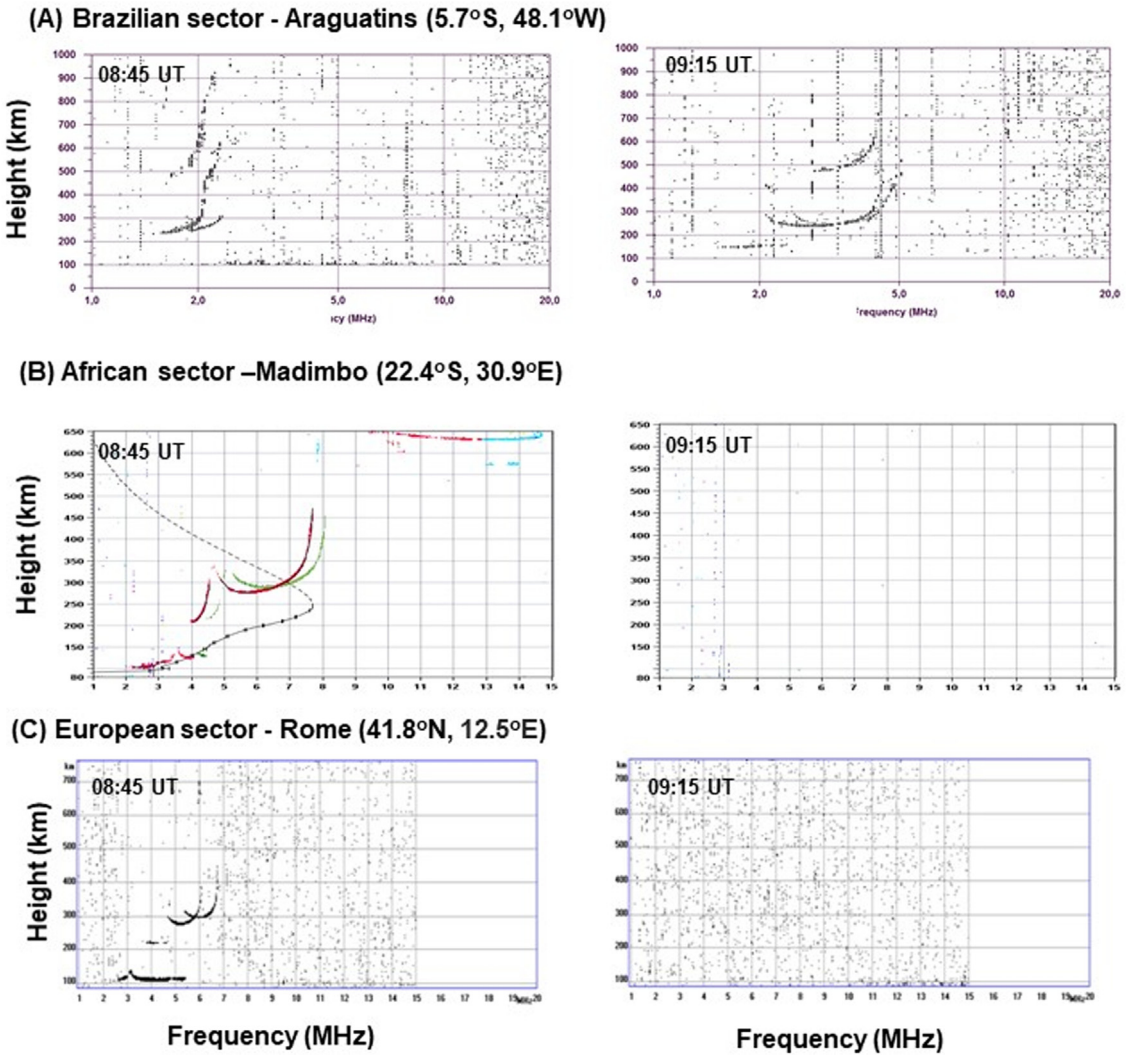


Fig. 5. Snapshots of ionograms obtained at 08:45 UT (before the SF X2.2) and 09:15 UT (after the SF X2.2) on September 06, 2017 at Araguatins, Madimbo, and Rome, in the (A) Brazilian, (B) African, and (C) European sectors, respectively.

African sector is completely surprising, since it is usually expected that VTEC enhances during SF with respect to the quiet time mean (positive ionospheric disturbances), from the equatorial region to mid-latitudes. A possible explanation for the anomalous VTEC behavior in the African sector is the combination of electrodynamics (Fountain effect and Equatorial Ionization Anomaly-EIA) and SF effect, because this event took place at 08:57 UT (11:57–12:00 LT) when the strength of the fountain effect is getting strong and the EIA formation is underway. However, this anomalous VTEC behavior needs further investigation. It is noticed from Fig. 4C that, after the X2.2 SF the VTEC values from 09:00 UT to 12:00 UT are ~10% higher than those of the quiet time mean over the European dip latitudes from 32°N to 39°N. Beyond these dip latitudes, VTEC values after the X2.2 flare are similar to quiet time ones except for the station KRTV.

The ionograms recorded at 08:45 UT and 09:15 UT over the African and European sectors are shown in Fig. 5B and 5C respectively. It is observed from these ionograms that the E- and F-region traces are present before the occurrence of the X2.2 flare and they disappear after. This shows that the enhanced density due to X2.2 flare caused a significant absorption of ionosonde signals over the European and African sectors, while the absorption is not present over Brazilian sector (Fig. 5A) since it is in the non-illuminated region.

2.2.2. The ionospheric VTEC and ionosonde response due to the X9.3 solar flare

A perusal in Fig. 4A, 4B and 4C shows that the observed VTEC values are strongly disturbed after the X9.3 SF event (11:53 UT) over Brazilian, African, and European sectors. It is important to mention that, all presented stations are illuminated by the Sun during the flare and these stations are spanning from equator to low, mid and high latitudes.

The VTEC after the X9.3 SF peak event show higher values (positive ionospheric disturbances) compared to those of quiet time mean and these higher VTEC values last for several hours after the X9.3 SF event. However, the higher VTEC values strength and lifetime vary from one station to the other. This indicates that the ionospheric local electrodynamics is superimposing on the SF effects. It is also noticed from VTEC variations that the disturbances produced by X9.3 SF are more intense than the previous X2.2 SF. In order to evaluate the strength of disturbances, the VTEC average is calculated for each sector between 12:00 and 18:00 UT. It is found that the mean VTEC for the 10 Brazilian stations are around 20% and 41% higher than the quiet period for the west and east sectors, respectively. The mean VTEC for the African and European stations are approximately 19% and 18% higher during the SF time compared to the quiet periods, respectively.

The fact that the higher VTEC values (positive ionospheric disturbances) last for several hours after the X9.3 SF peak, it is probably related to the slow decay of the peaks in the X-ray and EUV flux variations (Fig. 2B and 2C). Surprisingly, considering the GPS receivers at equatorial and low latitudes, it is seen from Fig. 4A and 4B that the positive ionospheric disturbance in the Brazilian sector, after the X9.3 SF, is stronger than that in the African sector. The X9.3 SF took place at 11:53 UT that is at 08:00–09:00 LT over GPS receivers located in the Brazilian sector and at around 14:00–15:00 LT in the African sector.

Plasma upward and downward motions are mainly caused by ionospheric electric fields and currents and those during disturbed conditions can significantly differ from their quiet-day patterns at low and mid latitudes. This is due to a simultaneous action of two processes: the magnetospheric dynamo and the ionospheric disturbance dynamo (Blanc and Richmond, 1980).

The magnetospheric dynamo is caused by dynamic interactions between the solar wind and the magnetosphere. This mechanism gives rise to electrical currents, which along with their associated electric fields (called prompt penetrating electric fields) can reach the lower latitudes through the conducting ionosphere (Mannucci et al., 2005; Huang et al., 2007; Fejer et al., 2008; Zhao et al., 2008; Tsurutani et al., 2008). Anyhow, this is a process that plays a significant role when the IMF B_z is southward (Tsurutani et al., 2004), which is not the case (see Fig. 2).

The ionospheric disturbance dynamo instead is triggered by an energy input into the thermosphere that modify the global thermospheric circulation, altering the electric fields and currents that are produced by the ionospheric wind dynamo action for quiet conditions at low and mid latitudes (Fejer and Scherliess, 1995; Fejer et al., 2008; Nicolls et al., 2006, Li et al., 2018, Lei et al., 2018, Blagoveshchensky and Sergeeva, 2019, Imtiaz et al., 2020). Specifically, the polarity and duration of the electric fields related to the disturbance dynamo can cause uplifts and descents of the ionospheric plasma that are at the base of large-scale local time dependent increases and decreases of VTEC. According to Fejer et al. (2008) during equinox there is a disturbance dynamo upward drift (with a consequent movement of the plasma towards altitudes where the recombination rate is lower) that between 8:00 and 9:00 LT is larger than between 14:00 and 15:00 LT. Therefore, this could explain why the Brazilian sector shows VTEC variations larger than those characterizing the African sector.

However, other studies have noticed an increase in VTEC of the order of ~2–4 TECu in the whole sunlit ionosphere (mid-latitudes) after the X2.2 SF, and of the order of ~8–10 TECu and ~15–16 TECu after the X9.3 peak at mid- and low-latitudes, respectively. The increase in VTEC due to X9.3 flare lasted longer because of the slow decay of the solar flare emission. In addition, HF-radio wave propagation blackouts and deterioration were recorded in some location, for more details see Yasyukevich et al. (2018). Also, Zhang et al. (2019) analyzed the differential TEC values and observed a traveling ionospheric disturbance (TID) related with the SF X9.3 flare in the North American sector.

Further, the ionograms obtained at 11:45 UT (before the SF X9.3) and 12:00 UT (after the SF X9.3) on September 06, 2017 over Brazilian, African and European sectors are presented in Fig. 6A, 6B and 6C respectively. It is clearly noticed from this figure that the three different sectors show E and F-regions trace before the X9.3 SF, but after the SF at 12:00 UT the E and F-regions disappear showing a blank ionogram. This is a clear indication that a large area of the globe was affected by the SF and radio waves were fully absorbed by the D-region. A complete list of 14 ionosondes showing the start and end time intervals of the absorption due to the X2.2 and X9.3 SF is given in Table 3. It is observed that, just after the SF there was a total radio fadeout. Then it turned to a partial fadeout, with the highest frequencies echoes appearing first on ionograms, and finally the complete ionogram echo is reestablished. These observations demonstrate that solar flare events can disrupt the radio signals over a large geographical extent for a few hours, which is a severe problem for communication and navigation radio applications.

2.3. Equatorial Ionization Anomaly (EIA) space-time variations in the South American and African sectors

During the daytime at the geomagnetic equator, the F-layer presents a vertical uplift, due to a zonal eastward electric field (**E**). The equatorial F-layer vertical upward drift ($\mathbf{V}_z$) during daytime is given by $\mathbf{V}_z = (\mathbf{E} \times \mathbf{B})/B^2$, where **B** is the geomagnetic field, and therefore the ionospheric plasma moves upward and diffuses downwards along the magnetic field lines due to gravitational and pressure gradient forces (equatorial fountain effect). Because of this fountain effect, a portion of the ionospheric plasma around the equator is removed and deposited at low-latitudes, around $\pm 15°$ to $\pm 17°$ dip-latitudes. The EIA has been extensively investigated under quiet and disturbed geomagnetic condi-

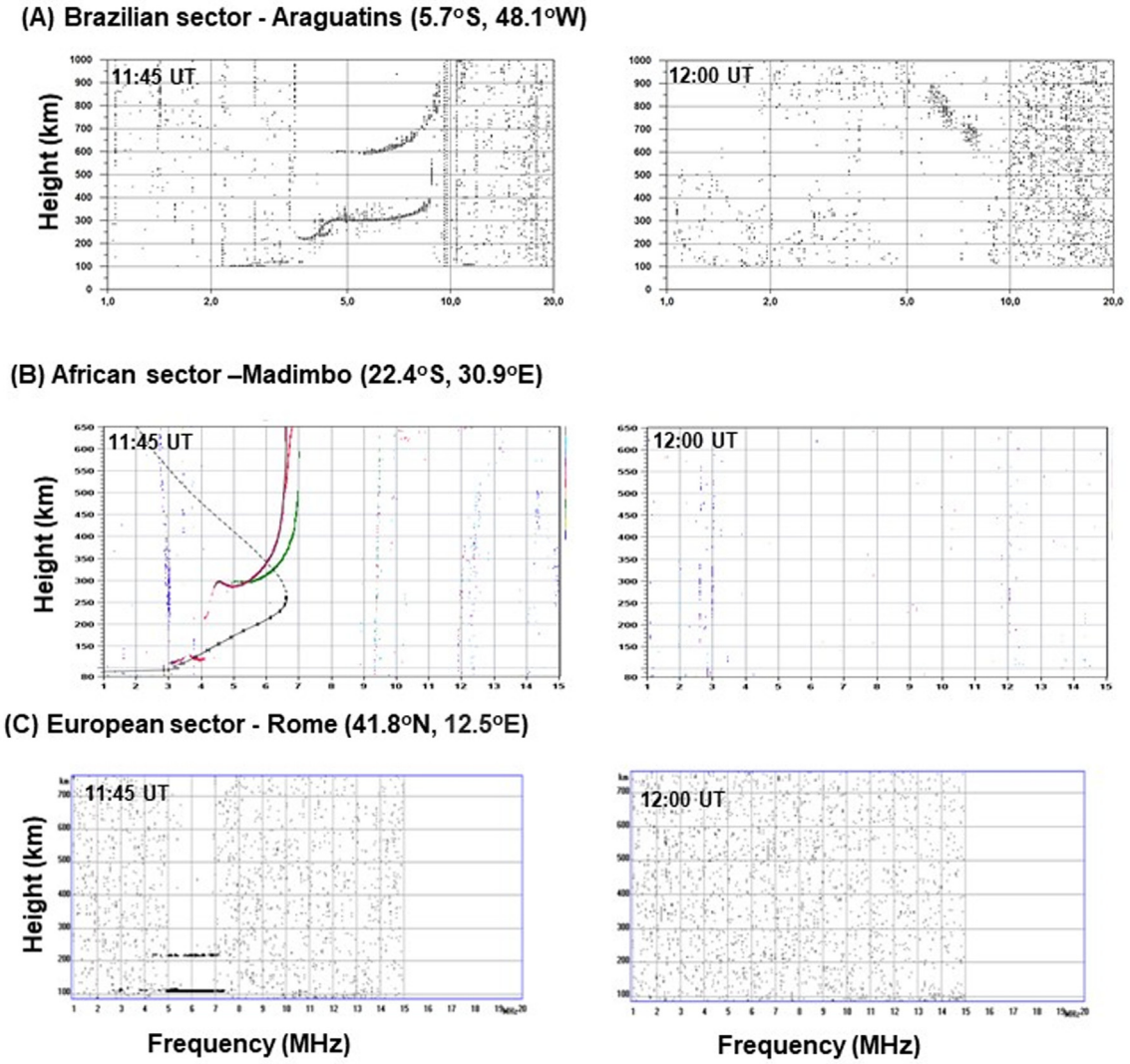


Fig. 6. Snapshots of ionograms obtained at 11:45 UT (before the SF X9.3) and 12:00 UT (after the SF X9.3) on 06 September 06, 2017 at locations Araguatins, Madimbo, and Rome in the Brazilian, African, and European sectors, respectively.

tions (Immel et al., 2006; Venkatesh et al., 2014, 2017; Fagundes et al., 2016; Eastes et al., 2019; Ribeiro et al., 2019; Vieira et al., 2017). Since SFs alter the electrodynamics occurred along with the EIA formation at the Earth´s illuminated side (daytime), it is interesting to investigate how the disturbances caused by the consecutive X2.2 and X9.3 SFs affected the formation and evolution of EIA in different sectors of the Earth, especially during the strongest SF event, where the soft X-ray, white-light emission (including UV and EUV), and γ-ray emissions increased in a rapid and really significant way.

As shown in the previous sections where we faced VTEC variations, the equatorial and low latitude regions of the Earth are the most disturbed regions by SFs. Thus, using the same methodology proposed by Venkatesh et al. (2014) and Fagundes et al. (2016), an investigation of the EIA in the Brazilian and African sectors is carried out to understand the impact of SFs on the EIA variability under this extreme condition. In addition, Swarm satellite measured in-situ electron density data (Friis-Christensen et al., 2006, 2008; Pezzopane and Pignalberi, 2019) are used to better understand the EIA evolution during the X2.2 and X9.3 events. For this purpose, the satellite orbits are considered on the quiet and disturbed days of September 05, 2017 and September 06, 2017, respectively.

The EIA variations over the Brazilian eastern and western sectors and African eastern sector are presented using a set of 20, 23, and 15 GPS stations, respectively, in Fig. 7 (Brazil) and Fig. 9 (Africa). As mentioned above, the X2.2 SF took place at 08:57 UT, that is nighttime in South American sector and daytime in the African sector. Nevertheless, the X9.3 event took place during daytime in South American and African sectors. The time when these events took place are indicated by dashed lines in Figs. 7 and 9 at 08:57 UT (X2.2, first dashed line) and at 11:57 UT (X9.3, second dashed line).

The EIA variations over Brazil in the east and west sectors are presented in Fig. 7A and B respectively. In this figure, the left panels represent the EIA variations during quiet day (September 05, 2017), while the right panels represent those on the flare day (September 06, 2017). Since it is dawn in the South American sector when X2.2 event took place, the VTEC has the lowest values during this time (dark blue, 0–5 VTECu). Consequently, some small changes caused due to SF X2.2 in VTEC are imperceptible for this local time (LT) when compared between the quiet and disturbed days.

The latitudinal profiles of the in-situ electron density observed by the Swarm satellites constellation over South America during X2.2 and X9.3 SF events are presented in Fig. 8A and B respectively. In these Fig. 8A and B, the first row shows measurements on the quiet day (September, 05 2017), while the second row shows measurements on the disturbed day (September 06, 2017).

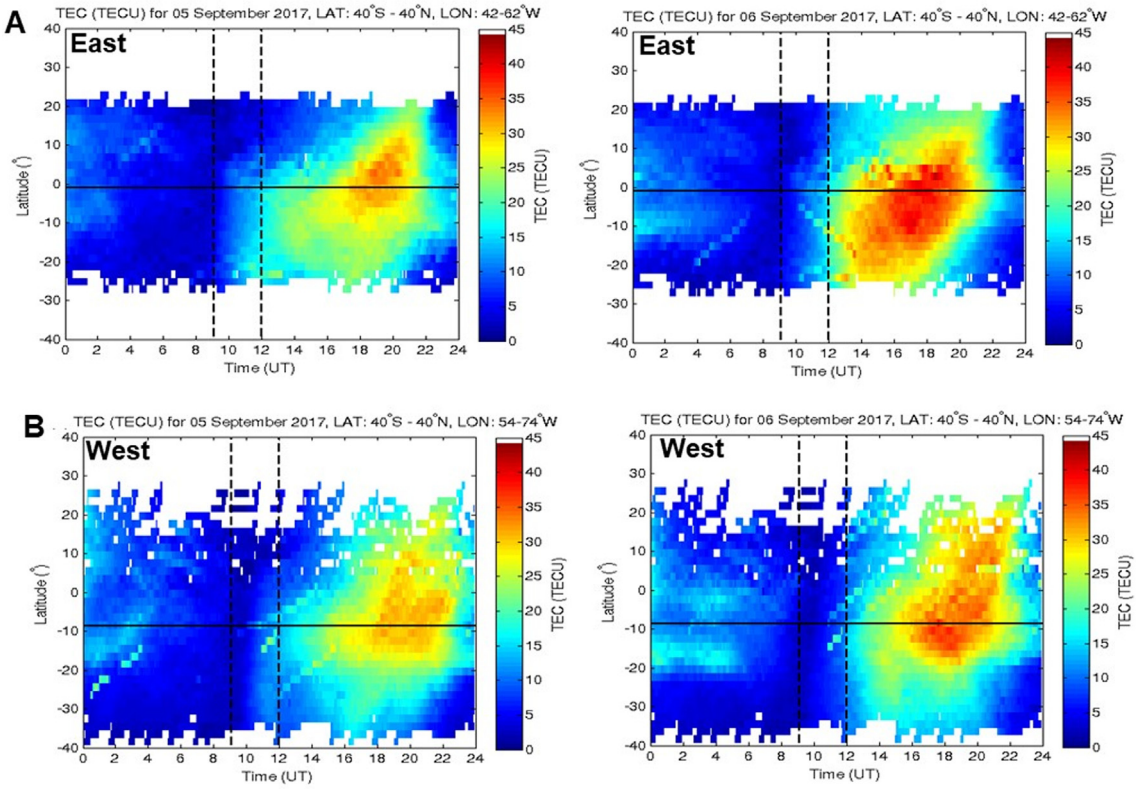


Fig. 7. (A) VTEC contour plots as a function of UT and latitude, showing the evolution of EIA in the eastern Brazilian sector (first row, 42°–62° longitudes) for September 05, 2017 and September 06, quiet and disturbed days, respectively. The two dashed vertical lines indicate the time of the occurrence of SFs and horizontal black line indicates approximate position of the magnetic equator. (B) The same as (A) but for the Brazilian western sector (second row, 54°–74° longitude).

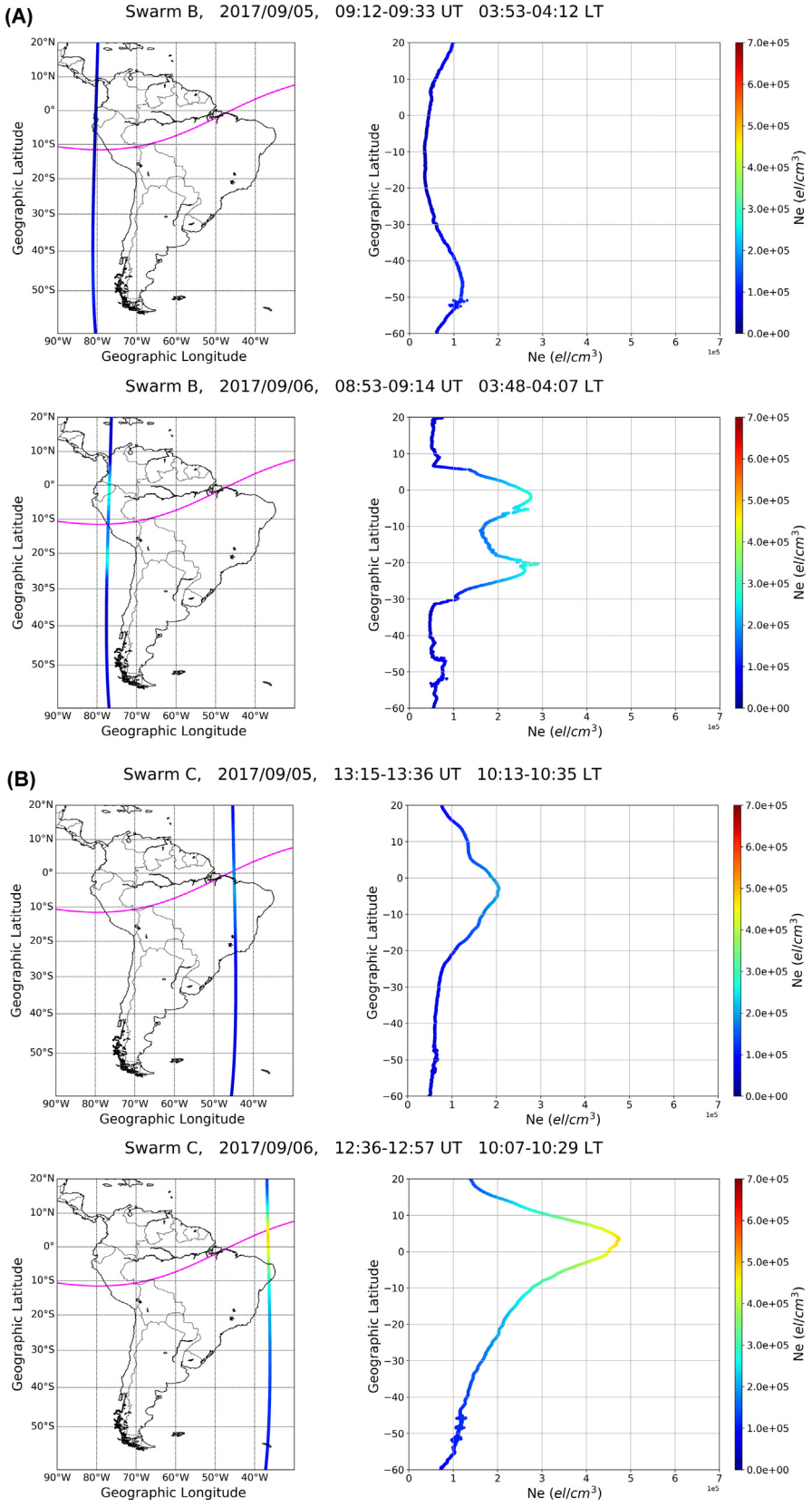


Fig. 8. In-situ electron density measurements in the South American sector from Swarm B on September 05, 2017 (quiet day) at 09:12 UT (03:53 LT) and on September 06, 2017 (disturbed day) at 08:53 UT (03:48 LT). (B) The same as (A) but for Swarm C on September 05, 2017 (quiet day) at 13:15 UT (10:13 LT) and September 06, 2017 (disturbed day), at 12:36 UT (10:07 LT).

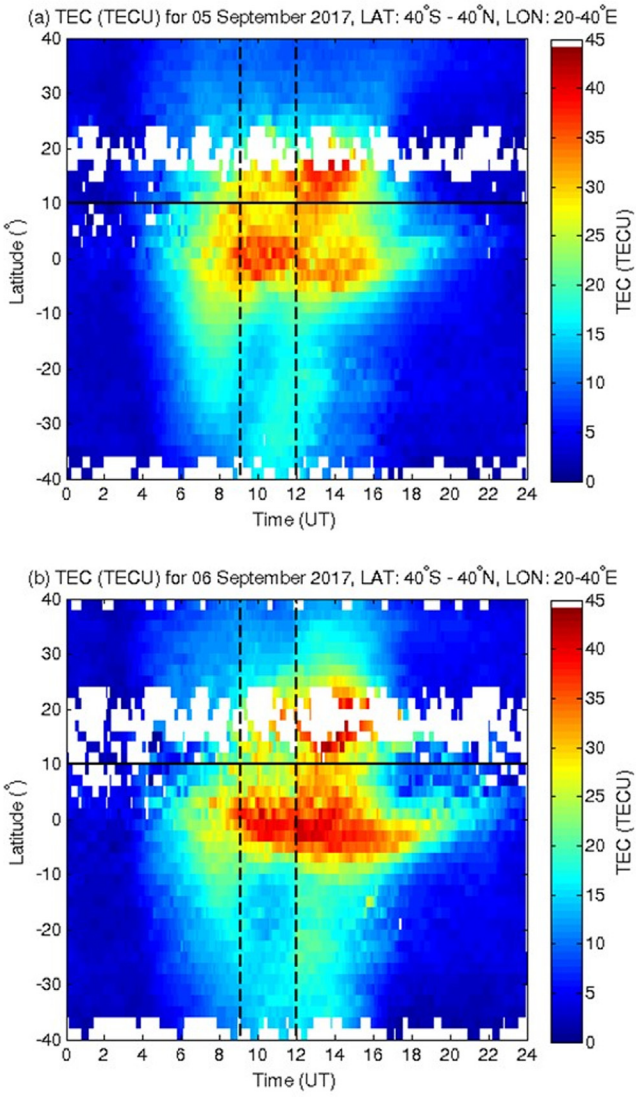


Fig. 9. (A) VTEC contour maps as a function of UT and latitude over the eastern African sector (first row, 20°–40° longitude) for September 05, 2017 quiet day. The two dashed vertical lines indicate the time of the occurrence of the SFs and horizontal black line indicates approximate position of the magnetic equator. (B) The same as (A) but for disturbed day (September 06, 2017).

Comparing Swarm in-situ observations between quiet and disturbed days just after the X2.2 event, it is noticed that the electron density has doubled just after the X2.2 event. As already mentioned, this event happened during nighttime in the South America and no change in electron density is expected. Since, these in-situ data were observed on consecutive days, also because the satellite latitudinal path and the time at which the observation was made are very similar. Also, doubling the in-situ electronic density cannot be related to the ionospheric day-to-day variability. Probably this change in the nighttime side is closely related to the X2.2 SF disturbance, via plasma transport from the dayside to the night-side, through thermosphere and ionosphere coupling. It may also be possible that, since the X2.2 occurred in the early morning in the Brazilian sector (05:57 LT), the ionosphere at Swarm satellite altitudes is sunlit and got exposed to the flare radiation resulting in a density enhancement at those particular heights. It is important to mention that VTEC is an integrated ionospheric parameter and it is very difficult to notice changes when VTEC values are small. On the other hand, the in-situ electron density observations from Swarm satellite can reveal changes at a specific height. This shows the importance of multi-instrument and multi-site observations to study space weather events and their effects at different scales.

It is seen from Fig. 7 that the X9.3 SF happened (around 12:00 UT) when the VTEC values in the South American sector present a transition from blue (10–15 TECu) to light blue (15–20 TECu). It should be mentioned that the X9.3 peak took place when the EIA was not yet formed. However, the X9.3 caused a rapid increase of X-ray and EUV fluxes around 12:00 UT which slowly decayed as seen in Fig. 2B and C. This SF event lasted for several hours and therefore the EIA was disturbed for several hours after the X.9.3 peak (see Figs. 4A and 7).

Comparing the left and right panels of Fig. 7A and 7B a VTEC intensification is clearly visible after the X9.3 SF in eastern and western sectors over Brazil. Thus, the EIA crest (reddish pattern in Fig. 7-right panels) after the X9.3 event (September 06) becomes stronger, larger and has a longer lifetime when compared to the previous day (September 05), indicating that the X9.3 SF had a major impact on the EIA in the American sector. It appears that the eastern sector was more affected than the western sector since the local time of the east sector is 1 h ahead of the west sector. One prominent feature of the EIA crest during the disturbed day is the latitudinal extension and lifetime in the east and west sectors. Fig. 7 shows that the EIA crest in the east sector is shifted southward ranging from −25° to 10° latitudes, while in the west sector is shifted northward, ranging from −15° to 20° latitudes. This should probably be closely related to the declination of the geomagnetic field and the distance between the geomagnetic and geographic equators.

Again, comparing the in situ electron density obtained from Swarm satellite data during quiet (September 05) and disturbed days (September 06) it is clear that the EIA trough and crests are not yet formed. However, the electron density has doubled after the X9.3 event in the eastern South American sector. The shape and latitudinal variation of the electron density for quiet and disturbed days are quite similar, but the maximum ionization is doubled around the geographic equator.

Further, using TEC observations on September 05 and 06, 2017 from a network of 15 GPS receivers (Table 2) in the African east sector, are presented in Fig. 9. The X2.2 and X9.3 SFs took place during local daytime and both flares disturbed the EIA daily variation over the African sector. Fig. 9 shows that, after the X2.2 peak, the southern EIA crest is just forming. The VTEC after the X2.2 SF peak (09:00–12:00 UT) increased at low-latitudes, indicat-

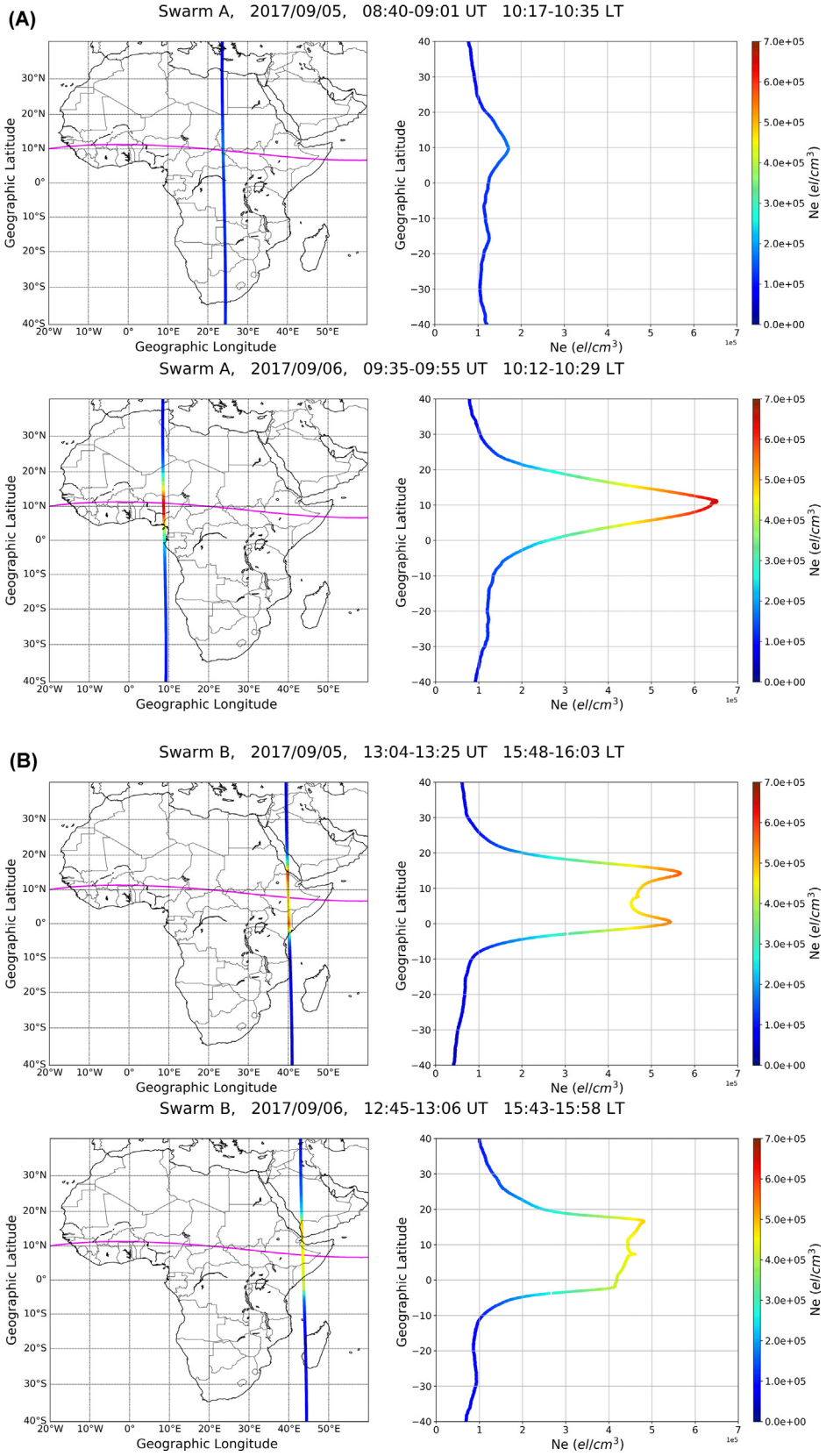


Fig. 10. (A) In-situ electron density measurements in the African sector from Swarm A satellite on September 05, 2017 (quiet day) at 08:40 UT (10:17 LT) and on September 06, 2017 (disturbed day) at 09:45 UT (10:12 LT). (B) The same as (A) but for Swarm B on September 05, 2017 (quiet day) at 13:04 UT (15:48 LT) and on September 06, 2017 (disturbed day) at 12:45 UT (15:43 LT).

ing an enhancement of the EIA southern crest compared with the previous quiet day (September 05, 2019).

Simultaneous in-situ observations from Swarm A satellite during the X2.2 and X.9.3 events are presented in Fig. 10A and 10B respectively. Fig. 10A shows that the electron density measured by Swarm increased by a factor of 4 on September 06 at 09:35 UT (10:17 LT) when compared to the previous quiet day at 08:40 UT (10:12 LT). Also, the latitudinal electron density profile is slightly different than that of the quiet day (Fig. 10A). It is important to mention that the orbits of Swarm A satellite on September 05 and 06 were around 25° and 10° longitudes, respectively. It is worth noting that at this moment the disturbance caused by the SF is more prominent since the electrodynamics related to the formation effect of the EIA was just starting. For this reason, the electron density increased by a factor of 4 and the change in the latitudinal profile structure is small.

The comparison between Fig. 9A and 9B shows that after the X9.3 SF (highlighted by the second dashed line) the EIA southern crest becomes stronger, broader in latitude and has a longer lifetime as compared with the quiet day (September 05, 2017). Also, a VTEC intensification beyond the EIA crest is observed in the northern and southern hemispheres. During the X9.3 SF peak, the fountain effect in the African sector is stronger than that in the South American sector (Fig. 7). This is due to the local time difference between the two sectors; in the African sector is around 14:00–15:00 LT, while in the South American sector is around 8:00–9:00 LT. Therefore, the combination of additional electron density produced by photoionization due to X9.3 SF and fountain effect gave rise to a stronger EIA in the African sector than in the American sector. It must also be noted here that the large enhancement in ΔH after X9.3 SF (Fig. 3) over the equatorial regions in the American and African sectors (related to an enhancement of EEJ) should have strengthened the EIA in these two sectors.

The in situ electron density during quiet day (September 05, 2017) measured by Swarm B (Fig. 10B, first row)) shows clear EIA trough and both crests well formed. However, on September 06, 2017 the EIA is disturbed, where the trough and crests have almost the same electron density (Fig. 10B, second row). The main difference between the quiet and SF disturbed days are the shapes of the latitudinal distribution of electron density and not the magnitude of the electron density.

3. Conclusion

This investigation is a contribution to the understanding of the equatorial-low-mid-latitudes ionospheric response to the extreme X2.2 and X9.3 solar flares that took place on September 06, 2017. In this paper, we have presented and discussed the impact of both solar flares on the ionosphere over South American, African and European sectors using magnetometer, GPS-VTEC, ionosonde, and Swarm satellite observations. The main findings of the present investigation are:

(a) The horizontal component of the geomagnetic field (H) in South American and African sectors are disturbed by both SFs. The X2.2 event took place in South American and African sectors during nighttime and daytime, respectively. In both sectors similar kind of ripples are recorded in the H component variations after the flare. This suggests that minor disturbances of the H component of the geomagnetic field due to solar flares can be observed in the non-illuminated side of the Earth as well.
(b) The X2.2 SF did not affect the VTEC and ionosonde records in the South American sector, because this sector was not illuminated by sun light during this flare. On the other hand, the European and African sectors were illuminated by sunlight and the X2.2 SF disturbed the VTEC and ionograms. However, in the African sector, it is noticed that the disturbed VTEC disturbances is higher in some regions and lower in other latitudes when compared with the quiet day. This anomalous VTEC behavior over the African sector can possibly be related to the combination of the beginning of the EIA formation and extra photoionization by the X2.2 SF.
(c) After the X9.3 SF peak, the VTEC is disturbed at all latitudes for several hours and ionograms experienced fade-outs for about one hour. The VTEC is around 20%, 41%, 19%, and 18% higher respectively in the east and west Brazilian sectors, African and European regions when compared with quiet day.
(d) The EIA in South America eastern and western sectors and African sectors is investigated using 3 networks of 20, 23, and 15 GPS stations, respectively. It is noticed that the EIA becomes stronger, larger and has a longer lifetime when compared to the previous quiet day. In addition, Swarm satellite constellation data are used to investigate the in situ latitudinal electron density profile to understand the EIA changes during these events. It is noticed that the electron density is doubled during the X2.2 SF and increased by a factor of 4 during the X9.3 SF when the fountain effect is not present or is still weak. However, the combination of SF and fountain effect changes the longitudinal profile of the in situ electron density.

Declaration of Competing Interest

The authors declared that there is no conflict of interest.

Acknowledgments

We wish to express our sincere thanks to the State of Sao Paulo Research Foundation (FAPESP) for financial

support through the process No 2019/09361-2 and Conselho Nacional de Desenvolvimento Científico e Tecnológico (CNPq) process No 302406/2017-4. One of the authors (KV) acknowledges the National Atmospheric Research Laboratory (NARL), India for support through fellowship. The authors wish to express their sincere thanks to the IBGE http://www.ibge.gov.br/home/geociencias/geodesia/rbmc/rbmc_est.php for providing dual frequency GPS data Brazil. C.M. Denardini thanks CNPq/MCTIC (Grant 303643/2017-0). The results presented in this paper rely on data collected at magnetic observatories. We thank the national institutes that support them and INTERMAGNET for promoting high standards of magnetic observatory practice (www.intermagnet.org). Also, geophysical, solar, and interplanetary data are provided by: http://wdc.kugi.kyoto-u.ac.jp/, http://omniweb.gsfc.nasa.gov/form/omni_min.html. The authors thank the European Space Agency (ESA) for making Swarm data publicly available via ftp://swarmdiss.eo.esa.int, and for the considerable efforts made for the Langmuir probes data calibration.

References

Bagiya, M.S., Thampi, S.V., Hui, D., Sunil, A.S., Chakrabarty, D., Choudhary, R.K., 2018. Signatures of the solar transient disturbances over the low latitude ionosphere during 6 to 8 September 2017. J. Geophys. Res. Space Phys. 1 (123), 7598–7608. https://doi.org/10.1029/2018JA025496.

Barta, V., Satori, G., Berenyi, K.A., Kis, A., Williams, E., 2019. Effects of solar flares on the ionosphere as shown by the dynamics of ionograms recorded in Europe and South Africa. Ann. Geophys. 37 (4), 747–761. https://doi.org/10.5194/angeo-37-747-2019.

Berdermann, J., Kriegel, M., Banys, D., Heymann, F., Hoque, M., Wilken, V., Borries, C., Hesselbarth, A., Jakowski, N., 2018. Ionospheric response to the X9.3 flare on 6 September 2017 and its implication tor navigation services over Europe. Space Weather 16 (10), 1604–1615. https://doi.org/10.1029/2018SW001933.

Blagoveshchensky, D.V., Sergeeva, M.A., 2019. Impact of geomagnetic storm of September 7–8, 2017 on ionosphere and HF propagation: A multi-instrument study. Adv. Space Res. 63 (1), 239–256. https://doi.org/10.1016/j.asr.2018.07.016.

Blanc, M., Richmond, A.D., 1980. The ionospheric dynamo. J. Geophys. Res. 85, 1669–1686.

Bruno, A., Christian, E.R., de Nolfo, G.A., Richardson, I.G., Ryan, J.M., 2019. Spectral analysis of the September 2017 solar energetic particle events. Space Weather 17, 419–437. https://doi.org/10.1029/2018SW002085.

Chamberlin, P.C., Woods, T.N., Eparvier, F.G., 2007. Flare Irradiance Spectral Model (FISM): daily component algorithms and results. Space Weather 5, S07005. https://doi.org/10.1029/2007SW000316.

Chamberlin, P.C., Woods, T.N., Eparvier, F.G., 2008. Flare irradiance spectral model (FISM): flare component algorithms and results. Space Weather 6, S05001. https://doi.org/10.1029/2007SW000372.

Chamberlin, P.C., Woods, T.N., Didkovsky, L., Eparvier, F.G., Jones, A. R., Machol, J.L., Mason, J.P., Snow, M., Thiemann, E.M.B., Viereck, R.A., Woodraska, D.L., 2018. Solar ultraviolet irradiance observations of the solar flares during the intense September 2017 storm period. Space Weather 16 (10), 1470–1487. https://doi.org/10.1029/2018SW001866.

Curto, J.J., Marsal, S., Blanch, E., Altadill, D., 2018. Analysis of the solar flare effects of 6 September 2017 in me the ionosphere and in the earth's magnetic field using spherical elementary current systems. Space Weather 16 (11), 1709–1720. https://doi.org/10.1029/2018SW001927.

de Abreu, A.J., Roberto, M., Alves, M.A., Abalde, J.R., Nogueira, P.A. B., Venkatesh, K., Fagundes, P.R., de Jesus, R., Gende, M., Martin, I. M., 2019. Effects of X2-class solar flare events on ionospheric GPS-TEC and radio waves over Brazilian sector. Adv. Space Res. 63 (11), 3586–3605. https://doi.org/10.1016/j.asr.2019.02.020.

de Castro, C.G.G., Raulin, J.P., Silva, J.F.V., Simoes, P.J.A., Kudaka, A. S., Valio, A., 2018. The 6 September 2017 X9 Super Flare Observed from Submillimeter to Mid-IR. Space Weather 16 (9), 1261–1268. https://doi.org/10.1029/2018SW001969.

Denardini, C.M., Chen, S.S., Resende, L.C.A., Moro, J., Bilibio, A.V., Fagundes, P.R., Gende, M.A., Cabrera, M.A., Bolzan, M.J.A., Padilha, A.L., Schuch, N.J., Hormaechea, J.L., Alves, L.R., Neto, P. F.B., Nogueira, P.A.B., Picanco, G.A.S., Bertollotto, T.O., 2018. The embrace magnetometer network for South America: first scientific results. Radio Sci. 53 (3), 379–393. https://doi.org/10.1002/2018RS006540.

Eastes, R.W., Solomon, S.C., Daniell, R.E., Anderson, D.N., Burns, A. G., England, S.L., Martinis, C.R., McClintock, W.E., 2019. Global-scale observations of the equatorial ionization anomaly. Geophys. Res. Lett. 46 (16), 9318–9326. https://doi.org/10.1029/2019GL084199.

Fagundes, P.R., Cardoso, F.A., Fejer, B.G., Venkatesh, K., Ribeiro, B.A. G., Pillat, V.G., 2016. Positive and negative GPS-TEC ionospheric storm effects during the extreme space weather event of March 2015 over the Brazilian sector. J. Geophys. Res. Space Phys. 121 (6), 5613–5625. https://doi.org/10.1002/2015JA022214.

Fejer, B.G., Jensen, J.W., Su, S.-Y., 2008. Seasonal and longitudinal dependence of equatorial disturbance vertical plasma drifts. Geophys. Res. Lett. 35 (20). https://doi.org/10.1029/2008GL035584.

Fejer, B.G., Scherliess, L., 1995. Time dependent response of equatorial ionospheric electric fields to magnetospheric disturbances. Geophys. Res. Lett. 22 (7), 851. https://doi.org/10.1029/95GL00390.

Friis-Christensen, E., Lühr, H., Hulot, G., 2006. Swarm: A constellation to study the Earth's magnetic field. Earth Planets Space 58, 351–358.

Friis-Christensen, E., Lühr, H., Knudsen, D., Haagmans, R., 2008. Swarm – An Earth observation mission investigating geospace. Adv. Space Res. 41, 210–216.

Immel, T.J., Sagawa, E., England, S.L., Henderson, S.B., Hagan, M.E., Mende, S.B., Frey, H.U., Swenson, C.M., Paxton, L.J., 2006. Control of equatorial ionospheric morphology by atmospheric tides. Geophys. Res. Lett. 33 (15). https://doi.org/10.1029/2006GL026161.

Imtiaz, N., Younas, W., Khan, M., 2020. Response of the low- to mid-latitude ionosphere to the geomagnetic storm of September 2017. Ann. Geophys. 38 (2), 359–372. https://doi.org/10.5194/angeo-38-359-2020.

Huang, C.-S., Sazykin, S., Chau, J.L., Maruyama, N., Kelley, M.C., 2007. Penetration electric fields: efficiency and characteristic time scale. J. Atmos. Solar-Terr. Phys. 69 (10), 1135. https://doi.org/10.1016/j.jastp.2006.08.016.

Lei, J.H., Huang, F.Q., Chen, X.T., Zhong, J.H., Ren, D.X., Wang, W.B., Yue, X.A., Luan, X.L., Jia, M.J., Dou, X.K., Hu, L.H., Ning, B.Q., Owolabi, C., Chen, J.S., Li, G.Z., Xue, X.H., 2018. Was magnetic storm the only driver of the long-duration enhancements of daytime total electron content in the Asian-Australian Sector Between 7 and 12 September 2017?. J. Geophys. Res. Space Phys. 123 (4), 3217–3232. https://doi.org/10.1029/2017JA025166.

Li, D., Kolokov, D.Y., Nakariakov, V.M., Lu, L., Ning, Z.J., 2020. Quasi-periodic pulsations of gamma-ray emissions from a solar flare on 2017 September 6. Astrophys. J. 888 (2), 53. https://doi.org/10.3847/1538-4357/ab5e86.

Li, W., Yue, J.P., Yang, Y., He, C.Y., Hu, A.D., Zhang, K.F., 2018. Ionospheric and thermospheric responses to the recent strong solar flares on 6 September 2017. J. Geophys. Res. Space Phys. 123 (10), 8865–8883. https://doi.org/10.1029/2018JA025700.

Liu, J.Y., Lin, C.H., Tsai, H.F., Liou, Y.A., 2004. Ionospheric solar flare effects monitored by the ground-based GPS receivers: Theory and Observation. J. Geophys. Res. Space Phys. 109, A01037. https://doi.org/10.1029/2003JA009931.

Liu, J.Y., Lin, C.H., Chen, Y.I., Lin, Y.C., Fang, T.W., Chen, C.H., Chen, Y.C., Hwang, J.J., 2006. Solar flare signatures of the Ionospheric GPS total electron content. J. Geophys. Res. Space Phys. 111, A05308. https://doi.org/10.1029/2005JA011306.

Lysenko, A.L., Anfinogentov, S.A., Svinkin, D.S., Frederiks, D.D., Fleishman, G.D., 2019. Gamma-ray emission from the impulsive phase of the 2017 September 6 X9.3 flare. Astrophys. J. 877 (2). https://doi.org/10.3847/1538-4357/ab1be0.

Mannucci, A., Tsurutani, B., Iijima, B., Komjathy, A., Saito, A., Gonzalez, W., Guarnieri, F., Kozyra, J., Skoug, R., 2005. Dayside global ionospheric response to the major interplanetary events of October 29–30, 2003 "Halloween storms". Geophys. Res. Lett. 32 (12). https://doi.org/10.1029/2004GL021467.

Nicolls, M., Kelley, M., Vlasov, M., Sahai, Y., Chau, J., Hysell, D., Fagundes, P.R., Becker-Guedes, F., Lima, W., 2006. Observations and modeling of post-midnight uplifts near the magnetic equator. Ann. Geophys. 24 (5), 1317. https://doi.org/10.5194/angeo-24-1317-2006.

Qian, L., Burns, A.G., Chamberlin, P.C., Solomon, S.C., 2011. Variability of thermosphere and ionosphere responses to solar flares. J. Geophys. Res. Space Phys. 116, A10309. https://doi.org/10.1029/2011JA016777.

Pezzopane, M., Pignalberi, A., 2019. The ESA Swarm mission to help ionospheric modeling: a new NeQuick topside formulation for mid-latitude regions. Sci. Rep. 9, 12253. https://doi.org/10.1038/s41598-019-48440-6.

Ribeiro, B.A.G., Fagundes, P.R., Venkatesh, K., Tardelli, A., Pillat, V.G., Seemala, G.K., 2019. Equatorial and low-latitude positive ionospheric phases due to moderate geomagnetic storm during high solar activity in January 2013. Adv. Space Res. 64 (4), 995–1010. https://doi.org/10.1016/j.asr.2019.05.032.

Sahai, Y., Becker-Guedes, F., Fagundes, P.R., Lima, W.L.C., de Abreu, A.J., Guarnieri, F.L., Candido, C.M.N., Pillat, V.G., 2007. Unusual ionospheric effects observed during the intense 28 October 2003 solar flare in the Brazilian sector. Ann. Geophys. 25 (12), 2497–2502. https://doi.org/10.5194/angeo-25-2497-2007.

Tsurutani, B., Mannucci, A., Iijima, B., Abdu, M.A., Sobral, J.H.A., Gonzalez, W., Guarnieri, F., Tsuda, T., Saito, A., Yumoto, K., et al., 2004. Global dayside ionospheric uplift and enhancement associated with interplanetary electric fields. J. Geophys. Res. Space Phys. 109 (A8). https://doi.org/10.1029/2003JA010342.

Tsurutani, B.T., Judge, D.L., Guarnieri, F.L., Gangopadhyay, P., Jones, A.R., Nuttall, J., Zambon, G.A., Didkovsky, L., Mannucci, A.J., Iijima, B., Meier, R.R., Immel, T.J., Woods, T.N., Prasad, S., Floyd, L., Huba, J., Solomon, S.C., Straus, P., Viereck, R., 2005. The October 28, 2003 extreme EUV solar flare and resultant extreme ionospheric effects: Comparison to other Halloween events and the Bastille Day event. Geophys. Res. Lett. 32 (3), L03S09. https://doi.org/10.1029/2004GL021475.

Tsurutani, B., Verkhoglyadova, O., Mannucci, A., Saito, A., Araki, T., Yumoto, K., Tsuda, T., Abdu, M., Sobral, J., Gonzalez, W., et al., 2008. Prompt penetration electric fields (ppefs) and their ionospheric effects during the great magnetic storm of 30–31 October 2003. J. Geophys. Res. Space Phys. 113 (A5). https://doi.org/10.1029/2007JA012879.

Tsurutani, B.T., Verkhoglyadova, O.P., Mannucci, A.J., Lakhina, G.S., Li, G., Zank, G.P., 2009. A brief review of "solar flare effects" on the ionosphere. Radio Sci. 44, RS0A17. https://doi.org/10.1029/2008RS004029.

Vieira, F., Fagundes, P.R., Venkatesh, K., Goncharenko, L.P., Pillat, V.G., 2017. Total Electron Content disturbances during minor sudden stratospheric warming, over the Brazilian region: a case study during January 2012. J. Geophys. Res. Space Phys. 122 (2), 2119–2135. https://doi.org/10.1002/2016JA023650.

Venkatesh, K., Fagundes, P.R., Seemala, G.K., de Jesus, R., de Abreu, A.J., Pillat, V.G., 2014. On the performance of the IRI-2012 and NeQuick2 models during the increasing phase of the unusual 24th solar cycle in the Brazilian equatorial and low-latitude sectors. J. Geophys. Res. Space Phys. 119 (6), 5087–5105. https://doi.org/10.1002/2014JA019960.

Zhang, S.R., Coster, A.J., Erickson, P.J., Goncharenko, L.P., Rideout, W., Vierinen, J., 2019. Traveling ionospheric disturbances and ionospheric perturbations associated with solar flares in September 2017. J. Geophys. Res. Space Phys. 124 (7), 5894–5917. https://doi.org/10.1029/2019JA026585.

Zhang, R.L., Liu, L.B., Le, H.J., Chen, Y.D., 2017. Equatorial ionospheric electrodynamics during solar flares. Geophys. Res. Lett. 44 (10), 4558–4565. https://doi.org/10.1002/2017GL073238.

Zhao, B., Wan, W., Liu, L., Igarashi, K., Nakamura, M., Paxton, L., Su, S.-Y., Li, G., Ren, Z., 2008. Anomalous enhancement of ionospheric electron content in the Asian-Australian region during a geomagnetically quiet day. J. Geophys. Res. Space Phys. 113 (A11). https://doi.org/10.1029/2007JA012987.

Zirin, H., 1988. Astrophysics of the Sun. Cambridge University Press.

Yan, X.L., Wang, J.C., Pan, G.M., Kong, D.F., Xue, Z.K., Yang, L.H., Li, Q.L., Feng, X.S., 2018. Successive X-class flares and coronal mass ejections driven by shearing motion and sunspot rotation in active region NOAA 12673. Astrophys. J. 856 (1). https://doi.org/10.3847/1538-4357/aab153.

Yasyukevich, Y., Astafyeva, E., Padokhin, A., Ivanova, V., Syrovatskii, S., Podlesnyi, A., 2018. The 6 September 2017 X-class solar flares and their impacts on the ionosphere, GNSS, and HF radio wave propagation. Space Weather 16, 1013–1027. https://doi.org/10.1029/2018SW001932.